International Journal of Marine Energy 14 (2016) 198–214

Contents lists available at ScienceDirect

International Journal of Marine Energy

journal homepage: www.elsevier.com/locate/ijome

Evaluation of the swirl characteristics of a tidal stream turbine wake

C.E. Morris *, D.M. O'Doherty, A. Mason-Jones, T. O'Doherty

School of Engineering, Cardiff University, Queens Buildings, The Parade, Cardiff CF24 3AA, UK

ARTICLE INFO

Article history:
Received 2 September 2014
Revised 20 July 2015
Accepted 11 August 2015
Available online 29 August 2015

Keywords:
Swirl
Flow characteristics
Tidal turbines

ABSTRACT

Tidal stream turbines (TSTs) produce a rotating downstream wake. This paper describes the characteristics of the swirl flow in the wake of a TST with a view of comparing these against classical swirl theory and investigating whether swirl is an important factor in wake recovery prediction.

Using computational fluid dynamics the paper describes the characteristics of velocities, pressure drop, viscosity and swirl number of 2, 3 and 4 bladed TSTs. To provide confidence in the results the characteristics are compared to the findings in the literature for a set of generic swirl generators. The swirl numbers for the TSTs in a 3.08 m/s tidal (plug) flow were found to be between 0.14 and 0.28, which describes a weak or very weak swirl flow. Whilst the characteristics are in agreement with theory it also means that the swirl component of the wake is not coupled with the axial component and cannot be used to estimate the wake length. However, peak swirl number for the 4 bladed turbine is close to the threshold of 0.3 at which axial velocity starts to become coupled with tangential velocity and therefore wake recovery may be related to S for some turbine designs.

* Corresponding author at: Cardiff School of Engineering, Cardiff University, Queen's Buildings, The Parade, Cardiff CF24 3AA, UK. Tel.: +44 (0)29 20 875905.

E-mail address: morrisce3@cf.ac.uk (C.E. Morris).

http://dx.doi.org/10.1016/j.ijome.2015.08.001
2214-1669/

Nomenclature

c'	constant rad/s
C	constant radm^2 s^{-1}
C'	constant m^2 s^{-1}
C_p	power coefficient
C_θ	torque coefficient
C_T	thrust coefficient
D	turbine diameter m
G_ϕ	axial flux of angular momentum kgm^2 s^{-2}
G_x	axial flux of linear momentum kgms^{-2}
p	static pressure Pa
r	radial distance m
R	turbine radius m
S	swirl number
u	axial velocity component ms^{-1}
U	free stream velocity ms^{-1}
v	radial velocity component ms^{-1}
w	tangential or swirl velocity component ms^{-1}
w_m	maximum tangential velocity component at a given x/D ms^{-1}
w_{m0}	maximum tangential velocity component within the flow field ms^{-1}
x	axial or downstream position m
Γ	circulation m^{2}s^{-1}
λ	tip speed ratio
ω	angular velocity rads^{-1}
Ω	vorticity s^{-1}
ρ	density kgm^{-3}

1. Introduction

1.1. Tidal Energy

It is widely understood and accepted that in order to ensure security of supply, the energy mix must diversify to include a wider variety of resources [1]. There is also a drive to reduce the emissions that contribute to global warming in an attempt to mitigate the effects of climate change. The current targets for the EU are set at a 20% reduction from the 1990 baseline level by 2020, with 20% of total energy consumption derived from renewable sources [2]. Each member state has an individual renewable energy target based on the proportion of energy provided by renewables when the targets were set and the potential for increasing this proportion. The UKs renewable energy target is 15% of the total annual energy consumption by 2020 [3]. In addition, the UK has also set a longer term target to achieve an 80% reduction in greenhouse gas emissions from the 1990 baseline level by 2050 [4]. Continued research and investment into emerging technologies and sectors which may not have a significant impact on the 2020 target is therefore vital if the UK is to meet its longer term objective.

Renewables such as wind and solar photovoltaic (PV), whilst providing a valuable contribution to the energy mix, are unpredictable in the medium to long term, presenting challenges to creating a reliable energy mix without advancements in and heavy dependence on energy storage technologies. The energy in the tides can be accurately predicted weeks, months and even years in advance. This predictability is the main advantage of tidal energy. Another advantage is the limited visual impact when compared with, for example, wind turbines.

One of the major advantages of tidal stream turbines (TSTs) is that they can be sized to suit the requirements of the local environment, i.e. coastal restrictions, tidal flow, tidal range, seabed topography, etc., and can be placed in either an individual or 'farm' configuration. As such, no large civil works are required and this method would therefore be less disruptive to wildlife, marine activity (and possibly the coastline) and would not present a significant barrier to water transport, compared to tidal range systems such as a barrage. There are a myriad of tidal stream turbines that are at various stages of development. However all the designs can be broadly grouped as either a horizontal or vertical axis tidal turbine. The Horizontal Axis tidal turbine (HATT) technology is the most advanced and is currently at the full scale prototype phase with much of the technology adapted from the wind industry.

The most advanced development towards installing full scale arrays, or farms, of tidal turbines is by Siemens Marine Current Turbines (MCT). They have, in partnership with ESB International, gained consent to install a 5 MW capacity array off the coast of Scotland at Kyle Rhea in the Western Isles by 2013 [5]. In addition, MCT are have consent to install a 10 MW array of turbines off Anglesey, Wales, UK, in 2016. The array will effectively consist of 5 Seagen *S* type twin rotor turbines over an area of 0.56 km^2, thus generating power for over 10,000 homes [6]. Further developments are being led by Tidal Energy Limited (TEL) who will be installing one of their DeltaStream units in the Ramsey Sound, off the coast of Pembrokeshire [7]. Furthermore a recent study in the Strangford Lough, by an independent science group led by Royal Haskoning and including the Northern Ireland Environment Agency, Queen's University Belfast, the Sea Mammal Research Unit and others, has shown that there were no adverse effects on the wildlife and environment following the installation of the SeaGen turbine within those waters [8]. This endorsement should provide impetus for the deployment of arrays of tidal devices by a number of companies. The density of the turbine distribution within an array will be determined by their overall environmental impact and their impact on each other, for both power and wake hydrodynamics. O'Doherty et al. [9] discussed the potential of an array of five 10 m diameter, three bladed turbines positioned in a triangular (equilateral) arrangement on a frame. Whilst the primary focus was on the loading on the whole structure, it was evident that the blockage caused by turbines positioned downstream of the upstream turbines caused the wakes to distort/bend around the downstream turbines.

An understanding of the drivers for the comprehension of wake size would therefore be a considerable benefit to the device designers for establishing the spacing requirements within an array of TSTs. This will also allow the environmental impact of such devices to be predicted prior to more in-depth design studies. It has been shown that high levels of turbulence can shorten the wake length and improve velocity recovery in the wake of a TST [10,11]. Proximity to the seabed has also been shown to affect the wake length [12,13]. This paper investigates whether the wakes of TSTs fit into classical swirl theory and determines if the swirl number can be used to estimate the length of wake recovery. The relationship between the number of blades and swirl was also considered. Whilst initial work focussed on the swirl characteristics of a 3 bladed turbine [14], this paper considers the swirl characteristics in the wake of 2, 3 and 4 bladed rotors.

1.2. Swirl flow

Swirl flows are observed in natural flows, such as tornadoes and typhoons, and have been widely used, for various reasons, in technical applications, such as aeronautics, heat exchange, spray drying, separation, combustion, etc. Their importance and complexity have been the subject of many research investigations for decades and a full review of the complex nature of the research into swirl and vortex breakdown can be found in Lucca-Negro and O'Doherty [15].

A swirl flow is defined as one undergoing simultaneous axial and vortex motions. It results from the application of a spiralling motion, a swirl velocity component (tangential velocity component) being imparted to the flow by the use of swirl vanes, axial-plus-tangential entry swirl generators or by direct tangential entry into a cylindrical chamber [16]. The *vorticity* of such flows is the curl or simply the distortion of the velocity field. This distortion, when it exists, results from the different angular velocities of different rings of particles. It therefore causes an object travelling on a circular path to rotate about its own axis as it goes along. The vorticity is defined as the ratio of the circulation round an infinitesimal circuit to the area of that circuit [17] and is given by:

$$\text{vorticity}\,\Omega = \frac{\text{circulation}}{\text{area}} = \nabla \times \underline{U_p} \tag{1}$$

where $\underline{U_p} = \underline{u} + \underline{v} + \underline{w}$, with the underline defining the gradient of each variable and the subscript p denoting an arbitrary point.

Flows with a tangential or swirl velocity w of type $w = C/r$ are called *potential* or *free* vortices. The vorticity of such flows tends to zero and the local flow rotates as a fixed body, that is, each element of the moving fluid undergoes no *net* rotation (with respect to chosen coordinate axes) from one instant to another. Hence such flows are called *irrotational*. Flows with solid-body rotation such that the tangential velocity is given by $w = c'r$ are called *forced* vortices. In this case the vorticity does not tend to zero and such flows are called *rotational*, that is each element of the moving fluid travels along a circular path and simultaneously rotates about its own axis [16].

In practice there may be rotational motion in one part of a flow field and irrotational motion in another part. In addition, all free vortices in real fluids have a central vortex core in which the vorticity is non-zero [16]. Conservation of angular momentum tends to create a free vortex flow, in which the circumferential velocity increases sharply as the radius decreases, w finally decaying to zero at $r = 0$ as viscous forces begin to dominate.

The free and forced vortices can be distinguished by the radial position of the maximum value of the tangential velocity component: in a free vortex, the maximum is found near the axis of symmetry while in the forced vortex, the maximum is found at the outer edge of the vortex. In some cases, a combined or Rankine vortex exists where the forced vortex equation is satisfied at small radial distances and the free vortex equation for large radial distances (Fig. 1). This type of vortex has been shown to develop, for example, when the flow is introduced tangentially at the periphery of a cylindrical chamber and exhausted at an axial nozzle [18–20]. The central forced vortex region exhibits flow field and turbulence characteristics, which appear to be significantly different from those seen in the surrounding irrotational vortex flow field. This central region is often referred to as the inner or vortex core. It is described as being shear free, but not vorticity free. The core is generally limited to that region of the solid-body rotating flow [21], but can also be extended to the radius of maximum tangential velocity.

The characteristics of each type of vortex can be uniquely defined as summarised in Table 1 [166].

In addition to classifying a swirl flow based on its type of vortex, it is common to characterise the degree or intensity of the swirl using the dimensionless local swirl number. This is because the degree of swirl has large-scale effects on the flow fields [166]. For example, introducing swirl into turbulent jets causes an increase in jet growth, rate of entrainment and rate of decay of the jet. The swirl number is defined as follows [22]:

$$S = \frac{G_\phi}{G_x r} \tag{2}$$

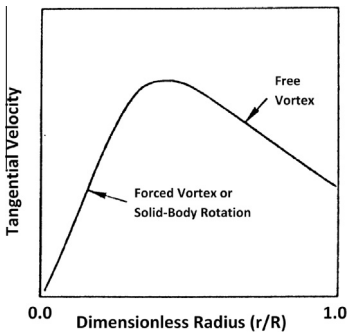

Fig. 1. Qualitative representation of a Rankine vortex [166].

Table 1
General characteristics of vortices.

	Forced vortex (solid-body rotation)	Free vortex (potential vortex)	Combined vortex (Rankine vortex)
Tangential velocity distribution w	wr^n = constant where $n < 0$	wr^n = constant where $n > 0$	$w = \frac{C'}{r}\left[1 - \exp\left(-\frac{r^2}{R^2}\right)\right]$
Angular velocity ω	c' (constant)	$\frac{C}{r^2}$ (function of r)	Function of radius
Circulation Γ	$2\pi\omega r^2$	$2\pi C$	$2\pi C'\left[1 - \exp\left(-\frac{r^2}{R^2}\right)\right]$
Vorticity Ω	4ω = constant	0	$\frac{4\pi C'}{R^2}\left[1 - \exp\left(-\frac{r^2}{R^2}\right)\right]$

where $r = R$, the TST radius since r is normally defined as the distance from the axis of rotation to the geometry edge. G_ϕ is the axial flux of angular momentum and is given by

$$G_\phi = \int_0^R (wr)\rho u 2\pi r dr = \frac{2}{3}\pi R^3 \bar{u}\bar{w} \tag{3}$$

G_x is the axial flux of linear momentum is given by

$$G_x = \int_o^R u\rho u 2\pi r dr + \int_0^R p 2\pi r dr = \pi\rho R^2 \bar{u}^2 \tag{4}$$

Assuming the static pressure is constant over the R, and consequently that the pressure term can be omitted [23].

The swirl number is typically used to define the level of swirl, such that very weak swirl is when $S \leqslant 0.2$, weak swirl corresponds to $0.2 < S \leqslant 0.5$ and strong swirl is when $S > 0.5$ [166].

A normalised swirl number (relative to the maximum swirl generated) can also be used to represent the data and is particularly useful as it can clearly show the level of the swirl and how it decays relative to the original level. This can be viewed by plotting the decay downstream of the TST against full recovery or as a downstream distance normalised to the maximum distance for a recovery to 90% of the upstream velocity.

2. CFD modelling

The operational performance characteristics of a 3 bladed TST which utilised a Wortmann FX 63-137 profile, with a 33° twist from the blade root to tip have previously been extensively studied [13,24,25]. The work discussed in this paper is derived from the modelling of 10 m diameter TSTs with 2, 3 and 4 blades, (Fig. 2) each with the same blade profile and twist and an average chord length of 1 m. The blade tip pitch angles were 3°, 6° and 9° for the 2, 3 and 4 bladed rotors respectively. These pitch angles were found to give maximum C_p in previous work.

In summary, the CFD domain was defined as a rectangular (sea) domain with a width and depth of 5D and a length of 40D to ensure the turbine was fully isolated from any boundary effects. The turbine was located 10D downstream from the inlet boundary such that its rotational axis was set at 35 m below the water. An axial aligned cylindrical domain (turbine) was subtracted from the rectangular domain to form a Multiple Reference Frame (MRF) with a non-conformal interface between the sea and turbine volumes which allowed the turbine to be rotated. The MRF was centred about the rotational axis of the turbine with a radius of 7 m and extended 0.5 m upstream and 1.5 m downstream. A quad meshing scheme was applied to the sea channel which incorporated ~ 0.5 M cells. Given the complex shape of the blades and geometry between the blades and the hub, the MRF volume was meshed with a tetrahedral hybrid scheme, incorporating ~1.5 million cells which provided a suitable cell size for grid independence for the characteristics discussed in this paper, based on previous work [13].

The seabed of the channel was modelled as a smooth wall using the no-slip boundary condition, while zero-shear was applied to the side and surface boundaries. The standard wall functions were

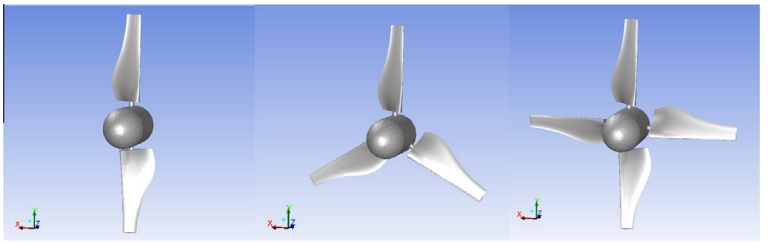

Fig. 2. Turbine configurations.

used in the near wall regions. In order to maintain an economical computational model, free surface interaction between the water and air was not included.

The RSM turbulence model was used, as shown by Mason-Jones [13,24] to give good agreement with experimental results for the 3 bladed rotor design.

For all the CFD models a water density of 1025 kg/m^3 and a dynamic viscosity of 0.00111 kg/ms were used. To model the upstream flow regime a plug flow velocity of 3.1 m/s was applied at the inlet with a turbulent kinetic energy of 1 m^2 s^{-2}. The turbulence was set above the desired value due to known problems of turbulence decay through the domain. At 1 turbine diameter upstream of the rotational plane of the turbine the turbulence intensity was around 10%, which has been shown to be realistic for a tidal stream site [26,27].

Experimental validation of a scaled turbine is described by Tedds et al. [25], using the same geometry as the 3 bladed turbine described in this paper, with non-dimensional scaling to a 10 m diameter turbine described by Mason-Jones et al. [24]. The turbine performance characteristics, that is the power, torque and axial thrust, have all been non-dimensionalised using Froude's Momentum Theory for an actuator disk, described by Myers and Bahaj [28,29]. The performance characteristics considered for this study are therefore presented in these non-dimensional forms, that is the power coefficient (C_p), the torque coefficient (C_θ) and the thrust coefficient (C_t) and are shown in Fig. 3.

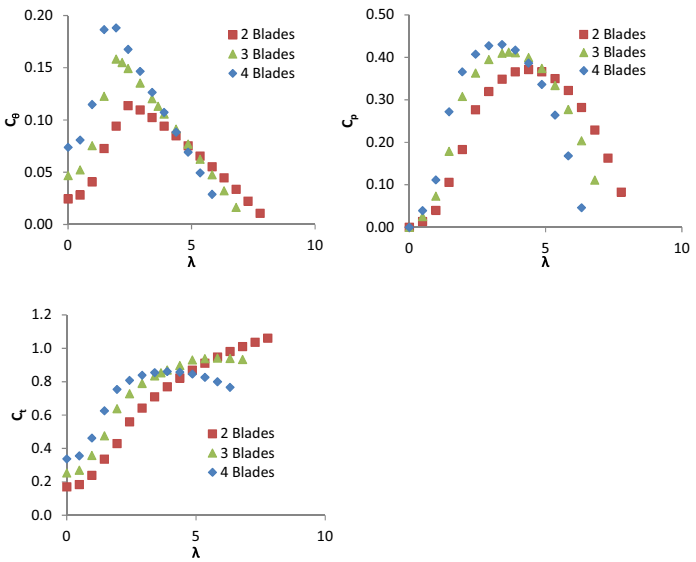

Fig. 3. Performance characteristics of the 2, 3 and 4 bladed turbines.

C_p is the ratio of the power extracted by the turbine to the available power from the tidal flow, as given by Eq. (5). C_θ is given by the ratio between the torque generated via the hydrodynamic lift and the maximum theoretical torque, as given by Eq. (6). C_T is given by the ratio between the axial thrust along the rotational axis of the turbine, generated via the hydrodynamic drag on the rotor blades and hub, and the axial thrust over the swept area of the turbine, as given by Eq. (7)

$$C_p = \frac{\text{Power}}{\frac{1}{2}\rho A v^3} \tag{5}$$

$$C_\theta = \frac{\text{Torque}}{\frac{1}{2}\rho A v^2 r} \tag{6}$$

$$C_t = \frac{\text{Thrust}}{\frac{1}{2}\rho A v^2} \tag{7}$$

What is clear is that there is an increase in peak torque, and peak power, with an increasing number of blades. There is also a reduction in the operational range and the λ at which peak power occurs. At the λ at which peak power occurs the thrust on each rotor is similar but at higher λ, the thrust on the 2 bladed rotor continues to increase whereas the thrust on the 3 bladed rotor remains almost constant and the thrust on the 4 bladed rotor decreases.

3. Swirl number

The swirl number was calculated using the second expression of Eq. (3) and (4). Fig. 4 shows how the Swirl number varies with λ and downstream distance for the 2 bladed turbine. Close to the turbine, at $x/D = 0.1$, the swirl varies with λ with a similar trend to that of C_θ, peaking at the same λ of 2.43, with a swirl number of 0.17. However, at very low values of λ, below 1, the swirl is in the same direction as the rotation of the turbine and the opposite direction to the flow further downstream of the turbine. This is due to recirculation zones behind the turbine blades which occur at very low rotational speeds. At all values of λ above 1, the swirl is highest at $x/D = 0.1$, decreasing with increasing downstream distance. At downstream distances between $x/D = 1$ and $x/D = 4$, the λ at which peak swirl occurs has increased to around 4, before decreasing with further increases in downstream distance, again reaching 2.43 at $x/D = 25$.

Figs. 5 and 6 show how the swirl number varies with λ and downstream distance for the 3 and 4 bladed turbines.

Close to the turbine, at $x/D = 0.1$, the swirl again varies with λ with a similar trend to that of C_θ, peaking at a swirl number of 0.23 for the 3 bladed turbine, and a swirl number of 0.28 for the 4 bladed turbine.

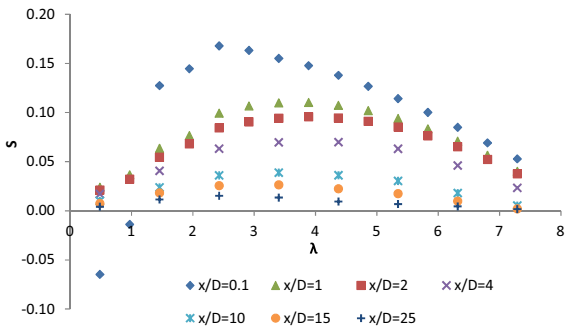

Fig. 4. Variation of swirl number with downstream distance for the 2 bladed turbine.

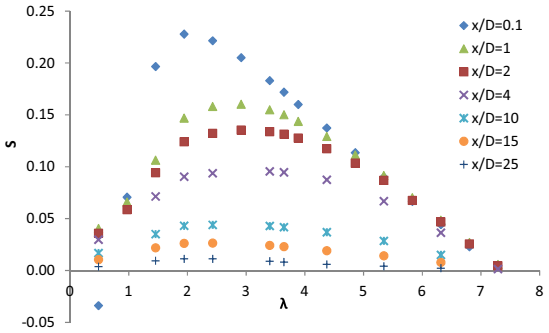

Fig. 5. Variation of swirl number with downstream distance for the 3 bladed turbine.

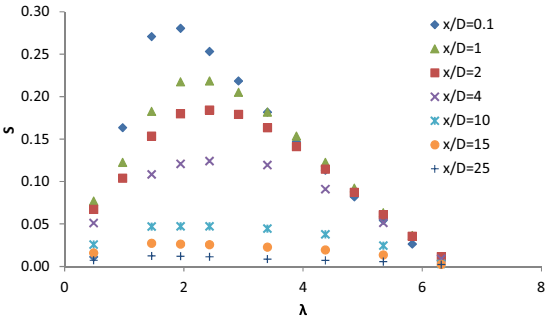

Fig. 6. Variation of swirl number with downstream distance for the 4 bladed turbine.

As with the 2 bladed turbine, at the lowest λ, 0.49, the swirl at $x/D = 0.1$ downstream of the 3 bladed turbine is in the same direction as the rotation of the turbine and the opposite direction to the flow further downstream of the turbine. However, unlike the 2 and 3 bladed turbines, even at the lowest λ, 0.49, the swirl at $x/D = 0.1$ downstream of the 4 bladed turbine is in the opposite direction to the rotation of the turbine and the same direction as the flow further downstream.

This is due to the reduction in size of the recirculation zones due to the increased blade pitch angle and the increase in positive swirl imparted to the flow due to the additional blades. Therefore, the relative effect of the recirculation zones is reduced.

For the 3 bladed turbine, at values of λ between 0.9 and 5, the swirl is highest at $x/D = 0.1$, again decreasing with increasing downstream distance. At values of λ above 5, the highest swirl no longer occurs at $x/D = 0.1$ but is instead further downstream, although the degree of swirl at $x/D = 0.1$, 1 and 2 is very similar. This is because, although the tangential velocity has reduced from $x/D = 0.1$ to $x/D = 1$, the axial velocity has also reduced (within the swept area of the turbine), and by a greater amount, so the ratio of angular momentum to linear momentum is higher. The same is true for the 4 bladed turbine, although it is found to occur over more of the operational range, at values of λ above 3. This is because the reduction in axial velocity increases with the number of blades due to a higher proportion of energy extraction.

The λ at which peak swirl occurs increases with downstream distance to around 3 at $x/D = 4$, for both the 3 and 4 bladed turbines, before decreasing with further increases in downstream distance, following the same trend as the 2 bladed turbine.

Fig. 7 compares the swirl number against λ at $x/D = 0.1$ for the 2, 3 and 4 bladed turbines. Maximum swirl number is shown to increase with the number of blades. The maximum calculated values of S are 0.17, 0.23 and 0.28 for the 2, 3 and 4 bladed turbines respectively, indicating that the turbine generates either a very weak swirl ($S < 0.2$) or weak swirl ($0.2 < S < 0.5$). This means that the tangential

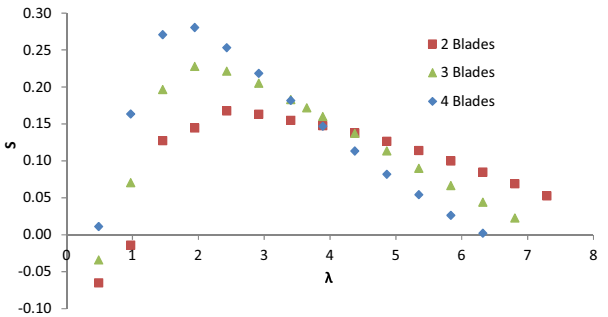

Fig. 7. Swirl Number vs λ at $x/D = 0.1$ for the 2, 3 and 4 bladed turbines.

component of velocity is decoupled from that of the axial velocity; hence the length of the wake cannot be inferred from knowledge of the swirl number. However, Gupta et al. [16] have shown that for a stronger swirl flow, i.e. $S \geqslant 0.3$ the tangential velocity starts to become coupled with the axial velocity, hence the stronger the swirl, the faster the decay in the wake length. The swirl number of the 4 bladed turbine is close to this threshold and therefore it is possible that for some turbine designs, the wake recovery will be related to the swirl number. C_θ, C_p and C_t have been shown to be independent of Re, and hence u, by Mason-Jones et al. [24]. However, since this work is based on a constant velocity, it is not possible to state whether S is independent of u from this particular study. Higher levels of swirl could therefore occur at different flow velocities.

Fig. 8 shows that the increase in peak S with number of blades is almost linear, although there is a slight reduction in the increase between 3 and 4 blades compared with the increase from 2 to 3 blades. This is to be expected since it is not feasible for the swirl number to increase linearly with a continually increasing number of blades.

At peak power the predicted swirl numbers again show an increase in S with the number of blades, as also seen in Fig. 8. Unlike at peak swirl, at peak power, there is a reduction in the rate of increase from 3 to 4 blades and the change in this rate is much greater. The greater change in rate at peak power is expected since there is a greater difference in λ for each turbine than at peak swirl.

3.1. Swirl decay

Fig. 9 compares the swirl decay for the λ which coincide with peak S, $\lambda = 2.4$ and peak C_p, $\lambda = 4.4$, for the 2 bladed turbine. At $\lambda = 2.4$ the swirl at $x/D = 0.1$ is higher, at 0.17, compared with 0.14 at $\lambda = 4.4$.

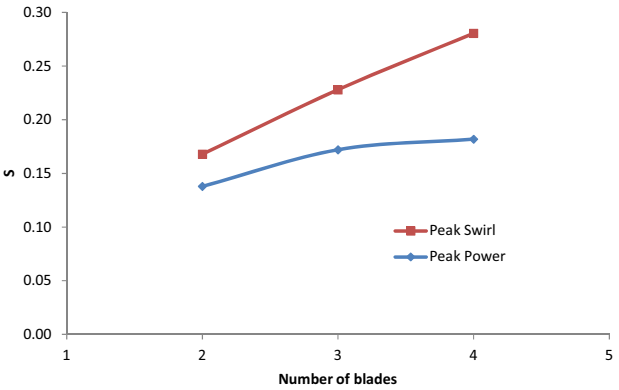

Fig. 8. Swirl number vs number of blades at peak swirl and peak power.

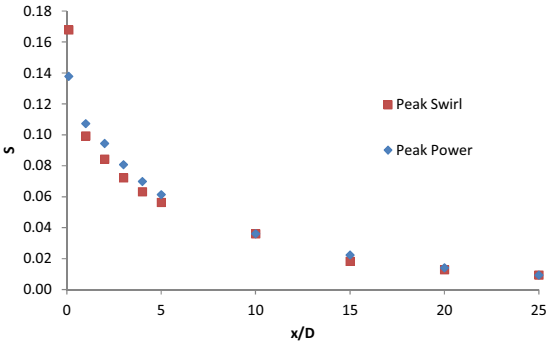

Fig. 9. Swirl decay at peak swirl and peak power for the 2 bladed turbine.

However, the initial decay in swirl is more rapid at $\lambda = 2.4$ and hence the swirl is lower for downstream distances between $x/D = 1$ and $x/D = 5$. At downstream distances above $x/D = 5$, the predicted swirl numbers are close for both values of λ and above $x/D = 15$ the differences between the predictions are negligible. This suggests that S is only affected, marginally, by λ in the near wake region.

Figs. 10 and 11 compare the swirl decay for the λ which coincide with peak C_θ and peak C_p, for the 3 and 4 bladed turbines.

At $x/D = 0.1$ downstream of the 3 bladed turbine, the swirl at peak power is 0.17 compared with a peak swirl of 0.23. For the 4 bladed turbine the swirl at $x/D = 0.1$ is 0.18, 0.1 lower than the peak swirl of 0.28. The difference between S at peak swirl and at peak power is therefore increasing with the number of blades meaning that S is more sensitive to λ at higher σ, as also shown by Fig. 12.

For the 3 bladed turbine the initial decay in swirl is again more rapid at peak swirl. However, unlike with the 2 and 3 bladed turbines, at peak power, the swirl downstream of the 4 bladed turbine shows very little decay at downstream distances close to the turbine. This is again because although the tangential velocity has reduced from $x/D = 0.1$ to $x/D = 1$, the axial velocity has also reduced, and by a greater amount, so the ratio of angular momentum to linear momentum is higher at $x/D = 1$. This occurs over more of the operational range for the 4 bladed turbine than for the 3 bladed turbine and does not occur within the operational range for the 2 bladed turbine as the 4 bladed turbine extracts the highest proportion of energy from the flow, and therefore has the greatest axial velocity deficit.

As with the 2 bladed turbine, other than immediately downstream of the turbine, the predicted swirl numbers are close at peak swirl and peak power for both the 3 and 4 bladed turbines. There is very little difference in S at downstream distances of $x/D = 1$ and above for the 3 bladed turbine

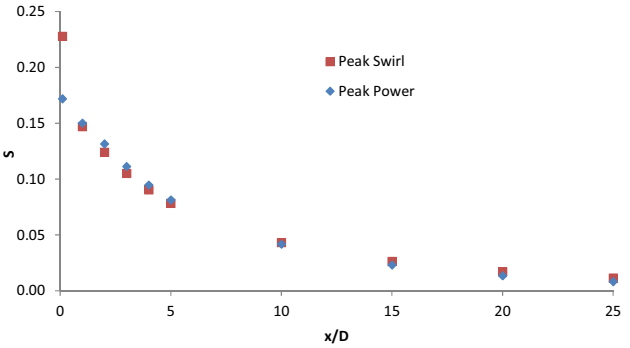

Fig. 10. Swirl decay at peak swirl and peak power for the 3 bladed turbine.

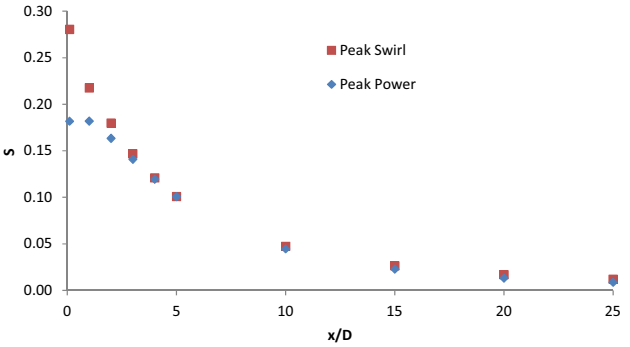

Fig. 11. Swirl decay at peak swirl and peak power for the 4 bladed turbine.

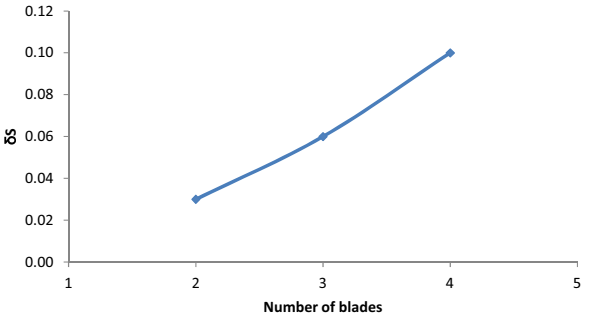

Fig. 12. Difference between peak swirl and swirl at peak power vs number of blades.

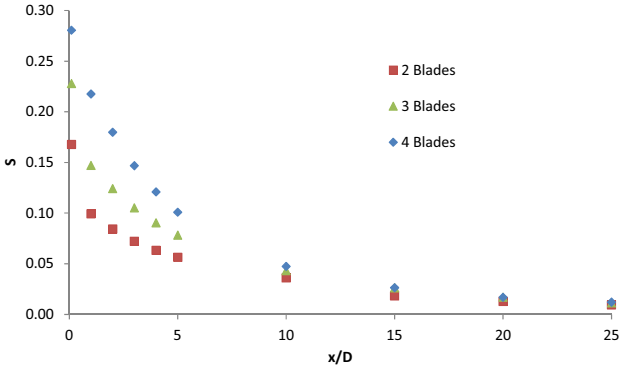

Fig. 13. Swirl decay at peak swirl for the 2, 3 and 4 bladed turbines.

and $x/D = 3$ and above for the 4 bladed turbine again suggesting that S in not dependent on λ outside the near wake region.

Fig. 13 compares the decay in swirl at the λ coinciding with peak swirl for the 2, 3 and 4 bladed turbines. It is clear that for all three turbines there is a rapid decay in swirl immediately downstream of the turbine, followed by a slow, steady decline. The peak swirl number is highest for the 4 bladed turbine and lowest for the 2 bladed turbine. This indicates that more tangential momentum is generated compared to the axial momentum when the number of blades is increased. However, the rate of

decay slows closer to the turbine for the 2 bladed turbine and further from the turbine for the 4 bladed turbine so that by $x/D = 10$ the values of S for each turbine are close and by $x/D = 20$ are approximately the same. Therefore the swirl number is only affected by the number of blades in the near wake region.

Fig. 14 shows that at peak power the swirl number is still highest for the 4 bladed turbine and lowest for the 2 bladed turbine. However, the difference between the peak swirl numbers has decreased from those at peak torque, with swirl numbers of 0.14, 0.17 and 0.18 for the 2, 3 and 4 bladed turbines respectively compared with 0.17, 0.23 and 0.28 at peak torque. S is therefore more dependent on σ in the near wake region at peak swirl than at peak power, due to greater differences in C_θ.

At downstream distances of $x/D = 1$ and above, similar trends to those found at peak torque are apparent, with the most rapid decay in swirl occurring for the 4 bladed turbine and the least rapid for the 2 bladed turbine. However, the decay in swirl from $x/D = 0.1$ to $x/D = 1$ is greatest for the 2 bladed turbine, with a smaller decay for the 3 bladed turbine and no decay for the 4 bladed turbine. As discussed above, this is because at higher rotational speeds there is a more rapid reduction in axial velocity than in tangential velocity between $x/D = 0.1$ and $x/D = 1$. This effect increases with the number of blades, as more energy is extracted from the flow.

4. Tangential velocity decay, W_m/W_{m0}

Overall flow characterisation of swirling flows is provided by Gupta et al. [16] based upon experimental time–mean data provided by Chigier and Chervinsky [30]. The work presents curves detailing the downstream decay and cross-stream profiles of axial and swirl velocities and static pressure. Swirling flows can be produced by a number of methods within industry and include a wide range of applications, i.e. swirl burners, cyclones, etc. However no matter what method used to produce the swirl, the characteristics seem to collapse onto reasonably well defined profiles. The findings of this work are no different to any swirl generator where the swirl number defines a very weak swirl as can be seen in Fig. 15, which superimposes the maximum tangential velocity at peak swirl and peak power for each turbine at each x/D, normalised to that at $x/D = 0.1$, onto the curves of Chigier and Chervinsky [30].

It should be reiterated at this point that the swirl decay being compared in this figure represent significantly different types of swirl generators, with the curve of Chigier and Chervinsky [30] based upon data from swirling jets as supposed to a turbine wake. That said; similarities can be seen between the decay in maximum tangential velocities of the turbine wake and jets. With D assumed to be the turbine diameter, the decay of the turbine wake swirl velocity maximum appears to replicate that of the jet very well, with the principle characteristics of an exponential fall when x/D is small and a subsequent slow but steady decline with increasing x/D. Furthermore the majority of this decay has occurred by $x/D = 5$.

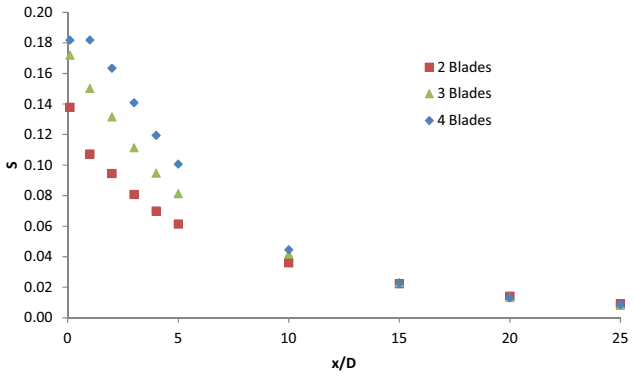

Fig. 14. Swirl decay at peak power for the 2, 3 and 4 bladed turbines.

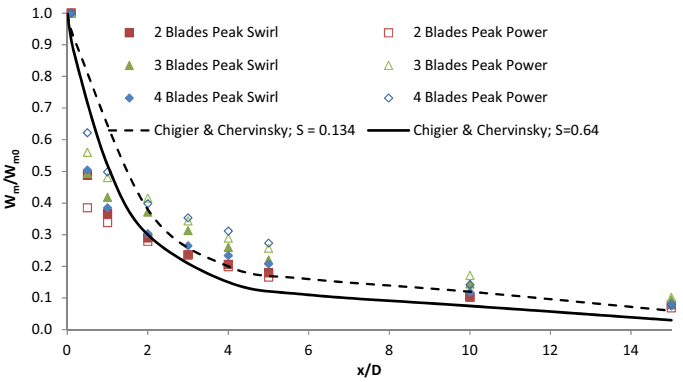

Fig. 15. Decay of maximum tangential velocity along axis of swirling jets (Chigier and Chervinsky, [30]) and in the wake of 2, 3 and 4 bladed turbines at peak swirl & peak power.

5. Type of vortex

Fig. 16 shows the tangential velocity profiles taken at $x/D = 1$ downstream of the 2 bladed turbine along a vertical line (y axis) and a horizontal line (x axis) at peak swirl and peak power. Maximum w is clearly higher at peak swirl than at peak power along both axes. At peak swirl maximum w along the y axis is higher than along the x axis but at peak power this is reversed as the area of maximum w rotates as the flow moves downstream and is closer to the x axis at peak power than at peak swirl, as shown in Fig. 17 (note: maximum tangential velocity given as negative since turbine rotation is defined as positive). This is because, although the maximum tangential velocity over the swept area is higher at peak swirl than at peak power, average axial velocity is also higher meaning the area of maximum w reaches the x axis further downstream. At both peak power and peak swirl, and along both axes, w increases from $r/R = 0$, reaches a maximum between $r/R = 0.35$ and $r/R = 0.55$ and then decreases to $r/R = 1.5$, showing a classical Rankine vortex profile. On the x axis, at r/R above 1.25, the tangential velocity becomes negative, indicating a small rotation in the opposite direction to that in the wake due to eddies shedding off the blades, before recovering towards 0 with increasing r/R. On the y axis, w remains close to 0 at r/R above 1.5.

Figs. 18 and 19 show the tangential velocity profiles taken at $x/D = 1$ downstream of the 3 and 4 bladed turbines along the y and x axes at peak swirl and peak power. As with the 2 bladed turbine, maximum w is higher at peak swirl than at peak power along both axes for both of the other turbine

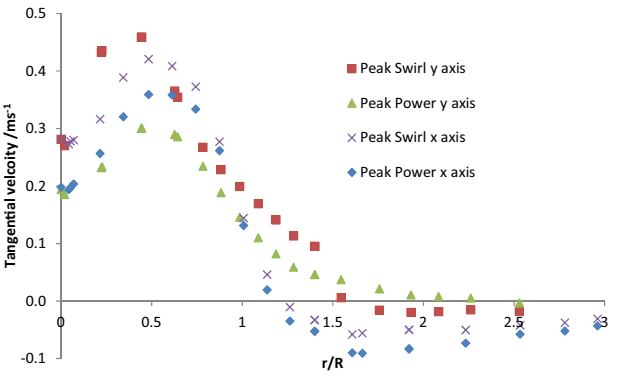

Fig. 16. Tangential velocity profile at $x/D = 1$ downstream of the 2 bladed turbine on x and y axes.

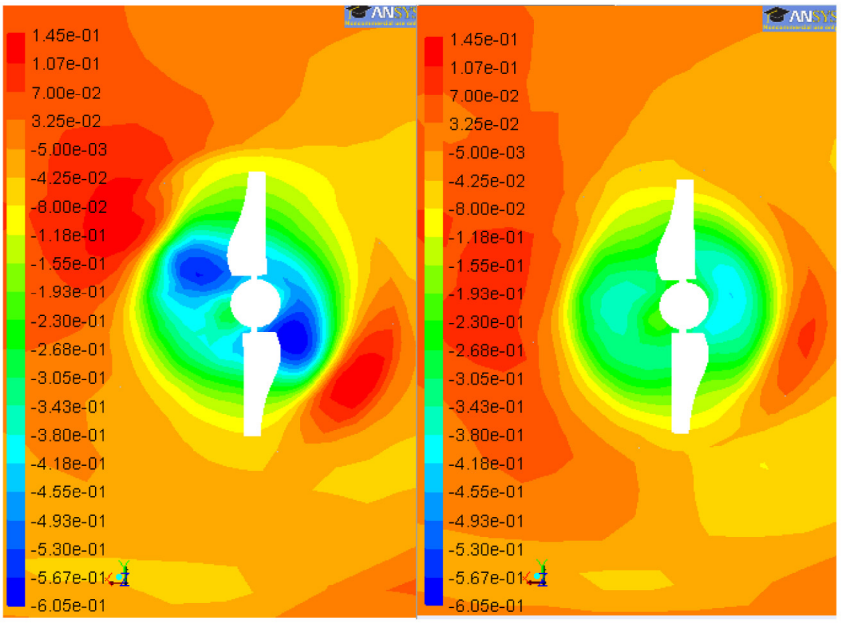

Fig. 17. Tangential Velocity Contours at $x/D = 1$ downstream of the 2 bladed turbine.

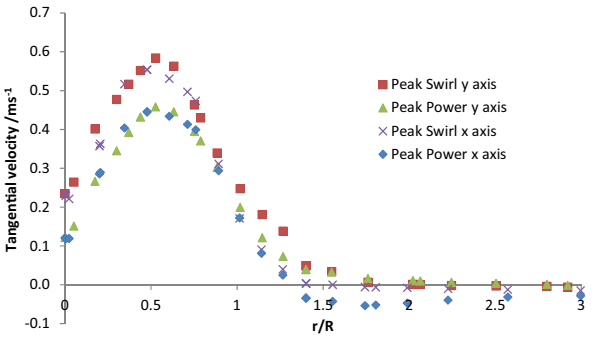

Fig. 18. Tangential velocity profile at $x/D = 1$ downstream of the 3 bladed turbine on x and y axes.

configurations. Unlike the 2 bladed turbine, there is little difference between the profiles along the x axis and the y axis for the 3 or 4 bladed turbine. This is because the blades are physically closer and therefore the tangential velocity profile becomes more uniform over the swept area of the turbine. The tangential velocity profiles follow the same trend as those of the 2 bladed turbine but there is less variation in the radial position at which maximum w occurs, which is around $r/R = 0.5$ for both the 3 and 4 bladed turbines at peak swirl and peak power along both axes. The profiles therefore demonstrate a Rankine vortex in the wake of each turbine at both peak swirl and peak power. Outside the wake region, at r/R above 1.5, w is close to 0 for both turbines.

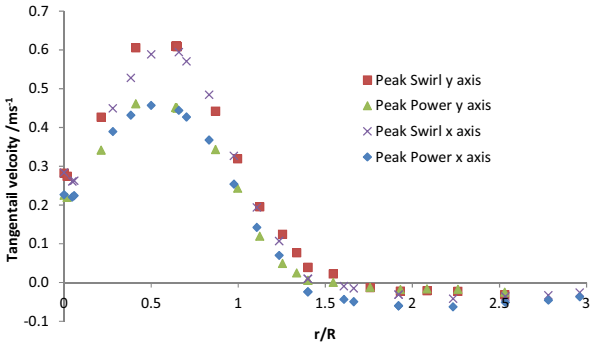

Fig. 19. Tangential velocity profile at $x/D = 1$ downstream of the 4 bladed turbine on x and y axes.

6. Dynamic pressure

It has been shown in this paper that the turbine generates either a very weak swirl or a weak swirl, depending on the number of blades, and it is known that very low swirl flows should result in a significant lateral (or radial), but a low axial, pressure drop [16]. To ensure that the results were in agreement with swirl theory for all three turbine configurations, the dynamic pressure was examined for the 2, 3 and 4 bladed turbines at λ at which peak Swirl occurred and at peak power since this is assumed to be the normal operating λ. Since the results at $x/D = 0.1$ were found to be heavily influenced by the hub, the pressure gradient in the radial direction was calculated at $x/D = 1$. The dynamic pressure at $x/D = 25$ was also extracted to enable the pressure gradient in the axial direction to be calculated. Fig. 20 shows the dynamic pressure profiles at $x/D = 1$ and $x/D = 25$ downstream of the 2 bladed turbine at peak swirl and peak power. Based on the data shown, at peak swirl the radial pressure gradient was calculated as 396 Pa/m and the axial pressure gradient was much smaller, at ~8.5 Pa/m. At peak power, the pressure gradient is much greater, at 814 Pa/m in the radial direction, compared with 7.3 Pa/m in the axial direction.

Fig. 21 shows the dynamic pressure profiles at $x/D = 1$ and $x/D = 25$ downstream of the 3 bladed turbine at peak swirl and peak power. At $x/D = 1$ at peak swirl average pressure drop of ~10.5 Pa/m in the axial direction. In the radial direction the pressure drop is ~560 Pa/m. By $x/D = 25$ the maximum pressure drop in the radial direction has reduced to ~110 Pa/m showing that the radial pressure drop is still dominant relative to the axial pressure drop.

At peak power the axial pressure gradient of 8.3 Pa/m. The radial pressure gradient is ~1050 Pa/m.

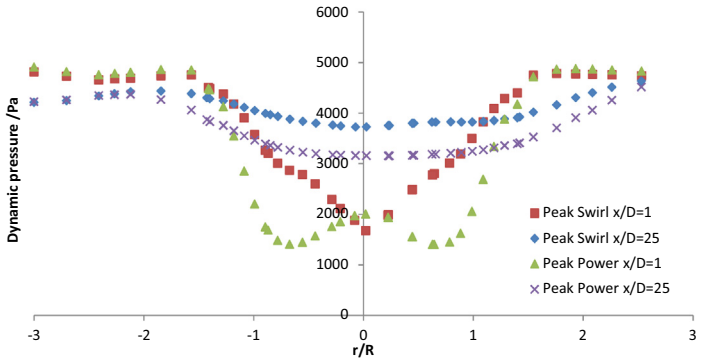

Fig. 20. Dynamic pressure profiles downstream of the 2 bladed turbine.

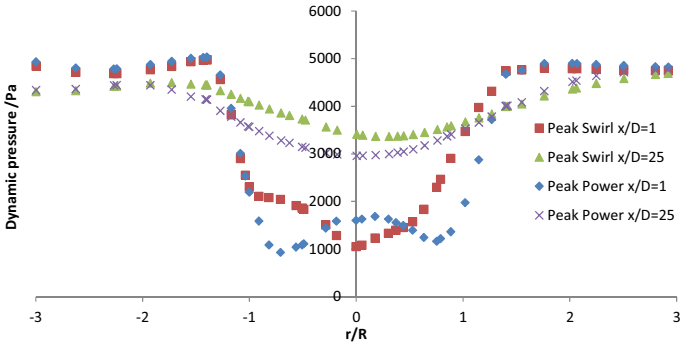

Fig. 21. Dynamic pressure profiles downstream of the 3 bladed turbine.

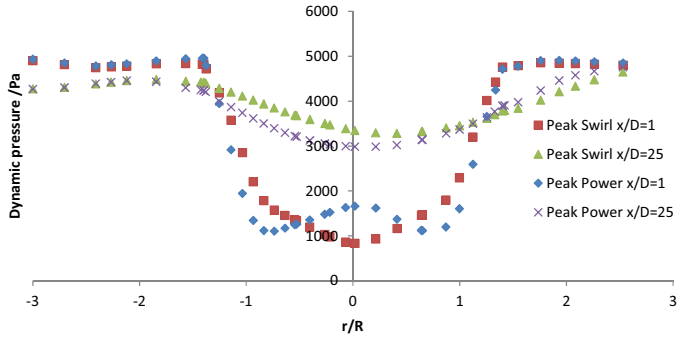

Fig. 22. Dynamic pressure profiles downstream of the 4 bladed turbine.

As with the 2 and 3 bladed turbines, the 4 bladed turbine also produces a wake with a much greater pressure gradient in the radial direction than in the axial direction. Fig. 22 shows gradients of 560 Pa/m and 10.2 Pa/m in the radial and axial directions respectively.

Again, at peak power, the pressure gradient in the wake of the 4 bladed turbine is much greater in the radial direction than the axial direction. From Fig. 22 the pressure gradient in the radial direction is 861 Pa/m. In the axial direction the pressure gradient is 7.8 Pa/m.

7. Conclusions

This paper investigated whether the wakes of TSTs fit into classical swirl theory and whether the swirl number can be used to predict wake recovery. The relationship between the number of blades and swirl was also considered.

It has been shown that close to the turbine, at $x/D = 0.1$, S varies with λ with a similar trend to the turbines C_θ, peaking at the same λ, for each of the turbine configurations. Further downstream, maximum S occurs at a λ which varies with x/D but follows the same trend for each turbine.

Peak swirl increases with the number of blades but is weak or very weak in all cases and therefore, for the rotor designs and flow velocity considered, swirl number cannot be used to predict wake recovery. However, peak S for the 4 bladed turbine is close to the threshold of 0.3 stated by Gupta et al. [16] at which axial velocity starts to become coupled with tangential velocity and therefore wake recovery may be related to S for some turbine designs. It is also possible that this may occur for this turbine design with a different mean flow velocity.

Swirl is only affected by the number of blades in the near wake region with values converging after $x/D = 10$.

Since the wakes of all three turbines, at both peak swirl and peak power compare well with the experimental work of Chigier and Chervinsky [30], demonstrate a classical Rankine vortex and follow the principle of a much greater pressure drop in the radial direction than in the axial direction it is reasonable to state that they fit classical swirl theory.

Future work will ascertain whether the swirl is affected by the flow velocity and could include other rotor designs with potentially higher swirl numbers.

Acknowledgements

The authors gratefully acknowledge the funding of the work discussed in this paper, provided by EPSRC and the Low Carbon Research Institute.

References

[1] DECC, UK Renewable Energy Roadmap Update 2013, Crown copyright, Department of Energy & Climate Change, London, 2013.
[2] European Union Committee, 27th Report of Session 2007–08 – The EU's Target for Renewable Energy: 20% by 2020, The Stationery Office Limited, London, 2008.
[3] DECC, UK Renewable Energy Roadmap, Crown copyright, Department of Energy & Climate Change, London, 2011.
[4] National Archives, 2008. Climate Change Act 2008 [Online]. Available at: <http://www.legislation.gov.uk/ukpga/2008/27/contents>, (accessed 15 Nov 2013).
[5] MCT, www.marineturbines.com, First Tidal Farm off Scotland's Isle of Skye: Marine Current Turbines secures site lease from The Crown Estate, April 2011, (accessed April 2011).
[6] SeaGeneration, www.seagenwales.co.uk, Sea Generation (Wales) Ltd., (accessed April 2014).
[7] Tidal Energy Limited, http://www.tidalenergyltd.com/, (Accessed October 2012).
[8] http://www.royalhaskoning.co.uk/en-gb/News/Pages/Seagen-Tidal-Turbine-Gets-All-Clear-From-Environmental-Scientific-Studies.aspx, Seagen Strangford Lough Tidal Turbine Gets All-Clear From Environmental & Scientific Studies, (accessed September 2012).
[9] T. O'Doherty, D.A. Egarr, A. Mason-Jones, D.M. O'Doherty, An assessment of axial loading on a 5 turbine array, Proc. Inst. Civil Eng. Energy 162 (EN2) (2009) 57–66. ISSN 1751-4223.
[10] P. Mycek, B. Gaurier, G. Germain, G. Pinon, E. Rivoalen, Numerical and experimental study of the interaction between two marine current turbines, Int. J. Mar. Energy 1 (2013) 70–83.
[11] C. Carlier, G. Pinon, B. Gaurier, G. Germain, E. Rivoalen. Numerical and experimental study of elementary interactions in marine current turbines array, in: EWTEC 2015–11th European Wave and Tidal Energy Conference, 2015.
[12] L.E. Myers, A.S. Bahaj, R.I. Rawlinson-Smith, M. Thomson. The effect of proximity upon the wake structure of horizontal axis marine current turbines, in: Proceedings of the 27th International Conference on Offshore Mechanics and Arctic Engineering, OMAE, 2008.
[13] A. Mason-Jones, Performance assessment of a horizontal axis tidal turbine in a high velocity shear environment (Ph.D), Cardiff University, 2010.
[14] C.E. Morris, A. Mason-Jones, D.M. O'Doherty, S.C. Tatum, T. O'Doherty, D.S. Thompson, Evaluation of the swirl characteristics of a tidal stream turbine wake, in: EWTEC 2013–10th European Wave and Tidal Energy Conference, 2013.
[15] O. Lucca-Negro, T. O'Doherty, Vortex breakdown: a review, Prog. Energy Combust. Sci. 27 (2001) 431–481.
[16] A.K. Gupta, D.G. Lilley, N. Syred, Swirl Flows, Energy and Engineering Science Series, Abacus Press, 1984.
[17] B.S. Massey, Mechanics of Fluids, eighth ed., Taylor and Francis, 2006 (Revised by J. Ward-Smith).
[18] J.J. Keyes, in: Proc. of the 1960 Heat Transfer and Fluid Mechanics Institute, Stanford, 1960.
[19] E.J. Roschke, J.J. Pivirotto, Jet Propulsion Lab. Tech. Report, no. 32-789, 1965.
[20] C. Sozou, J. Swithenbank, Adiabatic transverse waves in a rotating fluid, J. Fluid Mech. 38 (part 4) (1969) 657–671.
[21] D.G. Sloan, P.J. Smit, L.D. Smoot, Modelling of swirl in turbulent flow systems, Prog. Energy Combust. Sci. 12 (1986) 163–250.
[22] D.G. Lilley, Prediction of inert turbulent swirl flows, AIAA J. 11 (7) (1973) 955–960.
[23] O. Lucca-Negro, Modelling of swirling flow instabilities (Ph.D), University Wales Cardiff, 1999.
[24] A. Mason-Jones, D.M. O'Doherty, C.E. Morris, T. O'Doherty, C.B. Byrne, I. Owen, S.C. Tedds, R.J. Poole, Non-dimensional scaling of tidal stream turbines, Energy (2012), http://dx.doi.org/10.1016/j.energy.2012.05.010.
[25] S.C. Tedds, R.J. Poole, I. Owen, G. Najafian, A. Mason-Jones, C.E. Morris, T. O'Doherty, D.M. O'Doherty. Experimental investigation of horizontal axis tidal stream turbines, in: 9th EWTEC, Southampton, 2011.
[26] G. McCann, M. Thomson, S. Hitchcock, Implications of site-specific conditions on the prediction of loading and power performance of a tidal stream device, in: 2nd International Conference on Ocean Energy, Brest, 15–17 October 2008.
[27] E. Osalusi, J. Side, R. Harris, Structure of turbulent flow in EMEC's tidal energy test site, Int. Commun. Heat Mass Transfer 36 (5) (2009) 422–431.
[28] L.E. Myers, A.S. Bahaj, Experimental analysis of the flow field around horizontal axis tidal turbines by use of scale mesh disk rotor simulators, Ocean Eng. 37 (2009) 218–227.
[29] L.E. Myers, A.S. Bahaj, Near wake properties of horizontal axis marine current turbines, in: 8th EWTEC, 2009, Uppsala, Sweden.
[30] N.A. Chigier, A. Chervinsky, Experimental investigation of swirling vortex motion in jets, Fifth United States National Congress of Applied Mechanics, Minnesota, 1966, J. Appl. Mech. Trans. ASME Ser. E 3 (1967) 443–451.